ELSEVIER

Contents lists available at ScienceDirect

Biosensors and Bioelectronics

journal homepage: www.elsevier.com/locate/bios





Engineering Geobacter pili to produce metal:organic filaments

Eric Szmuc^a, David J.F. Walker^{a,c,f}, Dmitry Kireev^d, Deji Akinwande^d, Derek R. Lovley^e, Benjamin Keitz^b, Andrew Ellington^{a,*}

- ^a College of Natural Sciences, University of Texas at Austin, Austin, TX, 78712, United States
- ^b McKetta Department of Chemical Engineering, University of Texas at Austin, Austin, TX, 78712, United States
- c U.S. Army Engineer Research and Development Center, Environmental Laboratory, University of Texas at Austin, Austin, TX, 78712, United States
- ^d Cockrell School of Engineering, University of Texas at Austin, Austin, TX, 78712, United States
- ^e Department of Microbiology, University of Massachusetts-Amherst, Amherst, MA, 01003, United States
- f Bioconscientia LLC, Austin, TX 78712, United States

ARTICLE INFO

Keywords: Pili Bioelectronics Bioengineering Biohybrid Self-assembly Metal:organic

ABSTRACT

The organized self-assembly of conductive biological structures holds promise for creating new bioelectronic devices. In particular, *Geobacter sulfurreducens* type IVa pili have proven to be a versatile material for fabricating protein nanowire-based devices. To scale the production of conductive pili, we designed a strain of *Shewanella oneidensis* that heterologously expressed abundant, conductive *Geobacter* pili when grown aerobically in liquid culture. *S. oneidensis* expressing a cysteine-modified pilin, designed to enhance the capability to bind to gold, generated conductive pili that self-assembled into biohybrid filaments in the presence of gold nanoparticles. Elemental composition analysis confirmed the filament-metal interactions within the structures, which were several orders of magnitude larger than previously described metal:organic filaments. The results demonstrate that the *S. oneidensis* chassis significantly advances the possibilities for facile conductive protein nanowire design and fabrication.

1. Introduction

Geobacter sulfurreducens produces electrically conductive type IVa pili (Steidl et al., 2016; Ueki et al., 2020; Adhikari et al., 2016; Tan et al., 2016; Walker et al., 2019; Liu et al., 2021) that are involved in extracellular electron transfer (Reguera et al., 2005; Vargas et al., 2013; Ueki et al., 2018). The pili are composed of individual pilA protein monomers. Although no experimentally confirmed structure of *Geobacter* pili exists to date, computational model reconstructions (Malvankar et al., 2015) based on the type IVa pili of Pseudomonas aeruginosa (sharing 50% homology with Geobacter) suggest a densely packed core of aromatics responsible for electron conduction via π - π stacking (Ueki et al., 2018; Vargas et al., 2013), consistent with the core of aromatic amino acids present in electrically conductive archaellum (Walker et al., 2019). Electrons are hypothesized to be transported through single pili, reducing conduit scales to nanometer dimensions, making bioengineering of pili for the construction of nano/micro-scale electronic devices appealing - including emerging technological applications in configurable biological circuitry for computing; skin-mounted devices for electrochemical sensing (Liu, Fu, et al., 2020; Muskovich and Bettinger, 2012); and bio-based devices for energy transport and storage (Fu et al., 2020; Liu et al., 2020).

Pili from *G. sulfurreducens* have previously been modified to alter their electrical conductance (Tan et al., 2016; Ueki et al., 2020; Vargas et al., 2013; Tan, Adhidkari et al. 2017) and binding properties (Ueki et al., 2020). For example, PilA monomers in the *Geobacter* strains *metallireducens* and *sulfurreducens* have had their aromatics replaced by alanines, reducing conductivity (Ueki et al., 2018; Vargas et al., 2013). Conversely, pili in *G. sulfurreducens* have been altered to include more aromatic residues, yielding exceptionally conductive pili (Tan et al., 2016, 2017). Through these modifications, the conductivity of pili has been tuned over a range of greater than a million-fold (Lovley and Walker, 2019). Modifying the wild-type pilin gene to encode pilin with additional short peptides at the carboxyl end yielded pili with the added peptides displayed on the outer surface of the pili, providing opportunities to bind metals or interact with antibodies (Ueki et al., 2020).

However, *G. sulfurreducens* only grows well under strict anaerobic conditions and thus generating sufficient pili for study and scaling has

^{*} Corresponding author. MBB 3.424, 2500 Speedway, Austin, TX, 78712, United States. *E-mail address:* andy.ellington@austin.utexas.edu (A. Ellington).

proven difficult. Efforts to produce *G. sulfurreducens* pili in *E. coli* have been successful (Ueki et al., 2020), but expression of pili in *E. coli* currently requires growth on solid supports, again limiting total pilin production and making their harvest labor-intensive.

Shewanella oneidensis is a gram-negative, naturally electroactive species that can grow as a facultative anaerobe, similar to *E. coli. Shewanella* expresses its own type IVa pili in liquid culture (McLean et al., 2008; Thormann et al., 2004), and thus presents a very attractive alternative for scaling pili production. By engineering pili-nanoparticle interactions we were able to use the *Shewanella* platform to express, purify, and characterize novel metal:organic assemblies of pilins into filaments.

2. Materials and methods

2.1. E. coli and S. oneidensis bacterial strains and expression vectors

E. coli::∆fimA strain for synthetic expression of conductive pilin (Ueki et al., 2020) was modified with additional pilin peptide sequences. Original plasmid backbones (Kanamycin resistance) were digested at NdeI and SacI cut sites and Gibson assembly was performed utilizing PCR amplified GFP gene from pKAR2(Bhadra et al., 2021) in trans along with flanking 30bp regions added from primers (Table S2). Passed E. coli::∆fimA cells were made electrocompetent and electroporated at 1.7 keV in BIO-RAD pulsar along with Gibson assembly plasmids. Fluorescent colonies were labeled under new plasmid pESpGFP. Wild-type and mutant (Gold-binding (Au), Sulfhydryl (C), 6X His-tag (H)) pilA genes were ordered as gBlocks (IDT)(Table S3) with an additional NcoI cut site following pilA gene and harboring flanking terminal BsaI sites. pESpGFP backbones and insert gBlocks were digested with BsaI, ligated, and transformed into electrocompetent *E. coli::ΔfimA*. Resultant plasmids were labeled pESpWT, pESpAu, pESpC, pESpH, respectively.

pESpWT plasmid backbones were further modified utilizing primer pairs (Table S2) with PCR amplified *pilA* region of pESpAu and pESpC backbones. Transformations were performed in passed, electrocompetent *E. coli::*Δ*fimA*. Resultant plasmids were designated pESpW-TAu and pESpWTC.

Deletion of native pilin genes mshA, flgK, pilA, within S. oneidensis MR-1 genome and addition of Geobacter sulfurreducens pilA under native expression was performed to construct S. oneidensis:: $\Delta mshA\Delta flgK\Delta pilA + GsPilA$ ($\Delta 4$). Plasmids for heterogenous mutant pili assembly were transformed and expressed within this strain.

For plasmid construction, pCD24r1 (Dundas et al., 2020) backbones were amplified using PCR with primer pair (Table S2). Geobacter pilA was inserted as gene block (IDT)(Table S3) to create pESOpWT using golden gate. Vector inserts were created from primer pairs (Table S2) and pESpC, pESpH plasmids with PCR amplification. Golden gate assembly was used to combine elements for transformation into electrocompetent S. oneidensis:: 44 using BIO-RAD E. coli pulsar at 1.2 keV. Resultant plasmids (Kanamycin resistant) were designated pESOpC and pESOpH.

2.2. E. coli and S. oneidensis growth conditions

*E. coli::*ΔfimA was grown aerobically overnight from frozen stocks in lysogeny broth (LB) containing 50 μg/mL kanamycin at 37 °C with shaking and plated at 50 μL on 10 cm culture dishes containing M9 media amended with MgSO₄, CaCl₂, 20% glucose solution, 500 μM IPTG, 50 μg/mL kanamycin, 0.02% yeast extract, 0.01% peptone, 0.5% v/v glycerol, and solidified with 1.5% agar. Cultures were grown for 48 h at 30 °C prior to harvest.

S. oneidensis:: $\Delta 4$ cultures were grown aerobically overnight from frozen stocks in lysogeny broth (LB) containing 25 µg/mL kanamycin as appropriate at 30 °C with shaking and either diluted 1:50 into LB media or plated directly at 50 µL on 10 cm culture plates. For dilutions, cultures

were grown in LB (supplemented with antibiotic as appropriate) aerobically, with shaking at 30 °C until reaching OD $_{600}$ ~0.6 and then centrifuged at 4,000×g. Cells were resuspended in LM broth media (Thormann et al., 2004) enhanced with 0.68 mM CaCl $_2$, 500 μ M sodium lactate, and 100 μ M IPTG. Cultures were grown aerobically, with shaking for 1 h at 30 °C prior to harvesting. For plated cultures, cells from overnight growths were added directly to 10 cm culture plates containing LM media with 0.68 mM CaCl $_2$, 5 mM sodium lactate, 100 μ M IPTG, antibiotic as appropriate, and solidified with agar. Cultures were grown at 30 °C for 24 h prior to harvest.

2.3. Pili harvesting and purification

For plated and broth cultures, pili were harvested and purified utilizing saturated ammonium sulfate or 300kDa MWCO polyethersulfone (PES) membranes (Millipore Sigma) following previously described methods (Neuhaus et al., 2020; Ueki et al., 2020) with few modifications. For all methods, cells were initially resuspended in 0.15 M ethanolamine pH 10.5 with additional 5 mM EDTA (Invitrogen)(Banin et al., 2006). Samples were lightly vortexed until cells were thoroughly resuspended and allowed to incubate on ice for 10 min prior to shearing. It was noted that mutant pili purifications led to lower final sample concentrations, with most likely causative factor determined by TEM imaging to be sample aggregations leading to sample loss during cellular debris centrifugation. To remedy this, EDTA was added to initial purification buffer (0.15 M ethanolamine pH 10.5) to remove metal factors that may be inducing pili-pili aggregations, giving sufficiently successful results. Ammonium sulfate precipitations were resuspended in 0.15 M ethanolamine pH 10.5 and a second precipitation was performed at 10% ammonium sulfate, left at 4 °C overnight, and pelleted at 14,000×g. Following purification, both methods resulted in small ((NH₄)₂SO₄) to large (300k MWCO filtering) amounts of DNA aggregation within samples, necessitating further DNase treatment. This treatment was administered by first completely re-solubilizing purified pili in 0.01 M ethanolamine pH 10.5, followed by neutralization (~pH 7.6) through HCl addition along with appropriate metals incorporation before adding DNaseI. Treated samples were re-purified through 100 kDa centrifuge filters with multiple milli-Q H2O washes, resulting in final sheared pili samples sufficiently free of DNA as confirmed through nanodrop devises and EtBr agarose gel electrophoresis.

2.4. Pili assembly into metal-organic frameworks

For purified pili, samples were added to a final concentration of $\sim\!0.01~\mu g/\mu L$ in buffered solutions. Sulfhydryl containing pili for binding gold nanoparticles were resuspended into 20 mM MES pH6 + 20 mM NaCl, with either 1.4 nm (NanoGold^m), 5 nm, or 20 nm gold nanoparticles (Sigma Aldrich, OD 1 stabilized in 0.1 mM PBS) added at 1:50 v/v concentration. His-tag pili were resuspended into 20 mM HEPES pH 7.6 + 150 mM NaCl. NiCl $_2$ was added to sample solutions at final concentration of 10 μ M. His-tagged pili for interaction with 10 nm Ni-NTA conjugated gold nanoparticles (Nanoprobes) were resuspended into 20 mM HEPES pH 7.6 + 150 mM NaCl + 0.05% Tween20 buffer. All samples were kept incubated on ice.

Labeling of pili by 10 nm Ni-NTA conjugated gold nanoparticles was performed on *S. oneidensis::* $\Delta 4$ pESOpH vector cells. Frozen stock of *S. oneidensis::* $\Delta 4$ pESOpH was grown in LB broth aerobic at 30 °C with shaking overnight and diluted 1:50 into LB broth the following day under same conditions. Upon reaching OD₆₀₀0.6 cells were centrifuged at 4,000×g and resuspended into LM media containing 0.68 mM CaCl₂ and 500 μ M sodium lactate. The single sample was divided into 2 equivalents, with one receiving additional 100 μ M IPTG for the histagged peptide induction. Following 1 h aerobic, shaking at 30 °C growth in LM media, samples were centrifuged at 4,000×g at 4 °C and cell pellets washed and resuspended into chilled 20 mM HEPES pH 7.6 + 150 mM NaCl +0.05% v/v Tween20. Centrifuge and washing were

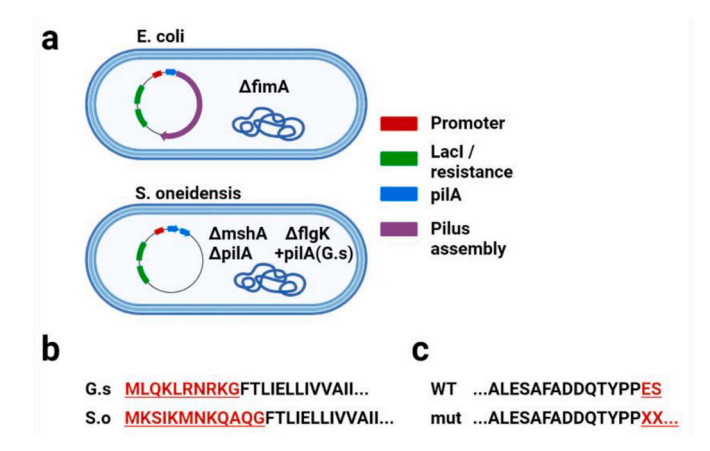


Fig. 1. Pili engineering for Shewanella oneidensis. (a) Genetic and plasmid engineering scheme for *E. coli* comparative to *S. oenidensis*::Δ4 (b) N-terminal cleavage domain (red underline) of *Geobacter sulfurreducens pilA* replaced with *Shewanella oneidensis* MR-1 native. (c) Mutants have PilA c-terminal glutamate and serine residues removed (red underline) to prevent charge interferences for specific targets.

repeated for another 2 rounds, with final resuspensions brought to an OD $_{600}$ 0.1.10 nm Ni-NTA conjugated gold nanoparticles (Nanoprobes) were added at a 1:25 v/v concentration to aliquots taken from final resuspensions. Cells were kept on ice during incubation with Ni-NTA gold nanoparticles.

TEM sample aliquots were placed on 300 mesh gold TEM grids,

stained by 2% uranyl acetate, and imaged on FEI Tecnai Transmission Electron Microscope (TEM) at 80 kV.

SEM electrodes were prepared by coating 4 nm platinum/palladium using Cressington mtm20 thickness controller connected with Cressington 208 Benchtop Sputter Coater and imaged using FEI Quanta 650 SEM

SEM sample aliquots were drop cast on center of 1×1 cm SiO $_2$ semiconductive wafers recently cleaned with 70% v/v isopropanol in water sonication bath for 5 min followed by milliQ H $_2$ O wash and N $_2$ blow dry under flame. Samples were coated with 1 nm iridium using Cressington mtm20 thickness controller connected with Cressington 208 Benchtop Sputter Coater and imaged using FEI Quanta 650 SEM equipped with Bruker EDX system. Elemental composition analysis was performed at 10 kV with 10 min total integration time on each sample.

2.5. 4-Probe electrical analysis

Electrodes were prepared by e-beam deposition of 20 μm of tungsten followed by 70 μm of gold. 4-probe ladders at 100 μm length and 2 μm gap sizes were placed on SiO₂ semiconductive wafers in circular orientation at ~1 mm diameter. Pili preparations from purifications were adjusted to ~20 $\mu g/\mu L$ (~2 mM). 1 μL of sample was drop-cast onto center of electrodes and allowed to air dry for 24 h in closed containers. Dried samples were washed with 30 μL of milliQ H₂O, blown dry with N₂, and again allowed to air dry for 2 h at room temperature prior to measurement. Electrodes were analyzed on a Cascade Summit HP4156C system set up with four probes conducting a dual sweeping voltage (I–V) curve from -650 mV to 650 mV sweep, 2 mV step, and 40 s hold with

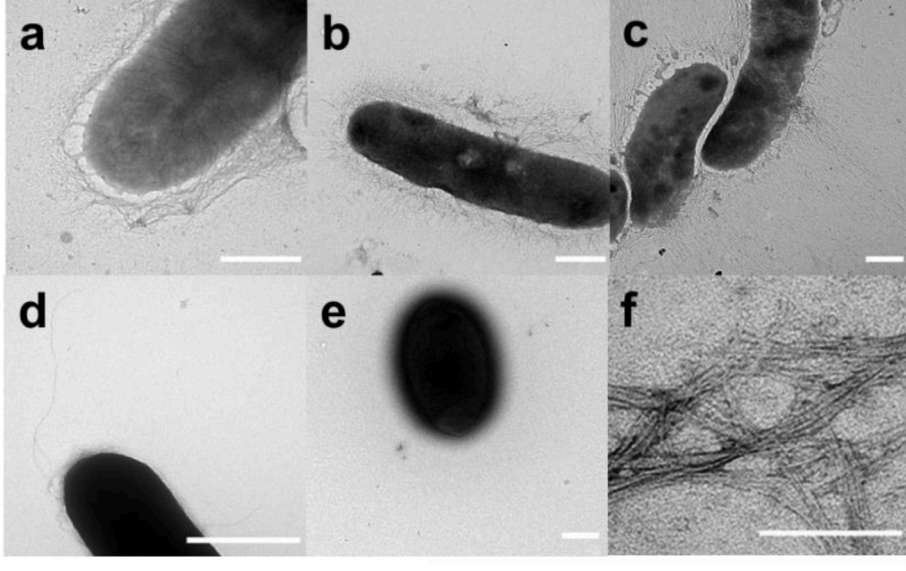
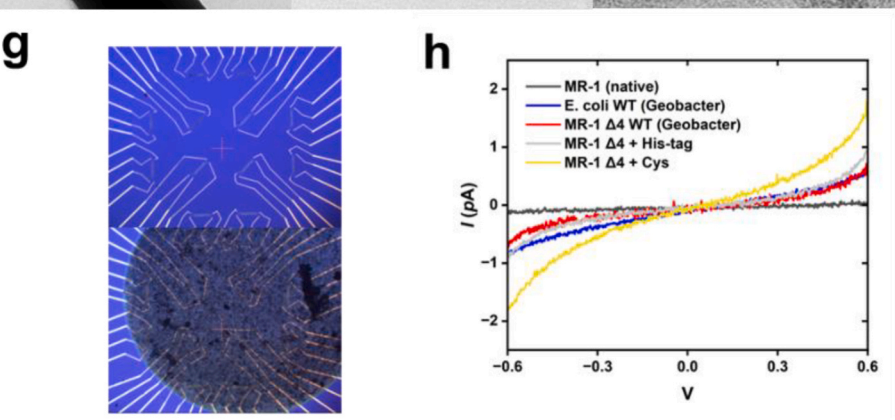


Fig. 2. S. oneidensis and E. coli conductive pili strains. (a) S. oneidensis::∆4 showing high numbers of wild-type Geobacter pili emanating from cell following broth culture expression. S. oneidensis:: 24 vector cells post induction and mutant pili expression: (b) pESpoC for binding gold nanoparticles (c) pESpoH containing 6X his-tag (d) S. oneidensis MR-1 following identical culture conditions, expressing visible native type IV pili and flagellum. (e) E. coli::ΔfimA strain following overnight culture and pili induction on minimal media plates (f) Isolated WT Geobacter pili loosely aggregating and showing minor bundling. (g) Electrode orientation blank and after sample drop cast (h) I-V conductance from voltage sweep performed on purified WT pili and mutants across strains. Scale bars 500 nm (a-e), 200 nm (f).



100 ms delay. Measurement values were obtained from current difference across the two inner electrodes. Variable source voltage was supplied at top electrode and removed by ground electrode at bottom. Sample measurements were carried out on 2 independent 4-probe ladders in triplicate. The average current-voltage response obtained over all measurements was fit to graph.

3. Results and discussion

3.1. Scaling and engineering pili expression

In order to engineer Geobacter pili, a convenient and efficient platform for pili expression was necessary. We initially attempted to produce Geobacter pili in E. coli (Ueki et al., 2020). Although production of the pili in E. coli was successful, the pili amounts obtained after isolation were regularly low, producing in our hands much less than the previously reported 1 mg/mL after harvesting multiple plates. We therefore turned to S. oneidensis for heterologous pili production, due to its ability to perform extracellular electron transfer (Bouhenni et al., 2010; Pirbadian et al., 2014), facultative anaerobic growth conditions (similar to E. coli), a similarity in pili production machinery, and a large and growing body of work on its genetic manipulation and bioengineering (Corts et al., 2019; Dundas et al., 2020; Suzuki et al., 2020). A S. oneidensis MR-1 strain, designated S. oneidensis:: \(\Delta 4 \), was constructed with a triple gene knock-out of MR-1 genes mshA, flgK, and native pilA (Fig. 1a). MshA is the main structural pilin in the mannose-sensitive hemagglutinin pilus, partially responsible for enabling biofilm formation (Saville et al., 2010). FlgK constitutes the flagella hook-filament junction protein essential for flagellar production (McCarter, 2001), and pilA belongs to the type IV pilus biogenesis genes and is upregulated during biofilm formation and attachment to electrodes (Rosenbaum et al., 2012). The Geobacter pilin gene (pilA) was introduced into the genome in place of the S. oneidensis pilA, and under the control of the native pilA promoter. The N-terminal cleavage domain of the Geobacter pilin (MLQKLRNRKG) was also swapped for the N-terminal cleavage domain (Fig. 1b) of S. oneidensis native PilA (MKSIKMNKQAQG) to enable correct cellular localization.

Pili were engineered to interact with gold nanoparticles by introducing additional peptide sequences at the carboxy terminus of PilA, which are solvent exposed when assembled into pili and thought to interact with metals in the environment (Reguera, 2018; Ueki et al., 2020). Two separate peptide extensions were introduced to bind gold nanoparticles: a 14 amino acid extension (-MHGKTQATSGTIQS (Brown, 1997);) that had a single methionine, and a 3 amino acid extension that (-ESC) that had a single cysteine. Engineered peptide sequences retained the native PilA proline turn motif that positions the carboxy terminal amino acids within the pili, but terminal glutamate and serine residues were removed while the new peptide tags were introduced (Fig. 1c). Only the -ESC addition could be produced in E. coli, as confirmed by SDS gel electrophoretic analysis and electron micrograph imaging. The lack of expression of the longer sequence is consistent with that fact that prior work had only yielded tags of 9 residues in length (Ueki, Walker et al. 2020). A 6X histidine tag was also engineered in-order-to assay affinity interactions with nickel-conjugated gold nanoparticles.

The engineered PilA variants were produced in a S. oneidensis:: $\Delta 4$ background (thus creating heterogeneous pili) to enable structural stability. The pilA variants were introduced on pCD24R1 (Dundas et al., 2020) under both native Shewanella promoter and LacI control (Fig. 1a), and pilin production was induced by IPTG.

As shown in Fig. 2, high pilin production was observed. Different strains harboring either no plasmid (Fig. 2a) or engineered pilA variants that had carboxy terminal extensions for -ESC (Fig. 2b) or a 6X his-tag (Fig. 2c) showed much more visible expression of pili than a previously developed *E. coli* strain (Ueki et al., 2020) that has also been shown to produce *Geobacter* pili (Fig. 2e). Indeed, in the engineered *S. oneidensis* strains (Fig. 2a–c) pili appear to aggregate around the cell

and extend tens of microns from the cell surfaces, in contrast to the native *S. oneidensis* MR-1 (Fig. 2d). This may be due in part a failure to retract and regulate pili growth, a phenomenon commonly seen with other type IVa pili produced heterologously (Giltner et al., 2012). The slightly elongated shape observed for *Shewanella* cells is likely due to arrested cellular division following the shift to low nutrient media.

3.2. Pili isolation and characterization

S. oneidensis has been previously shown to produce pili (leading to visible cellular aggregations) under aerobic, slightly oxidative growth conditions (McLean et al., 2008), and in the presence of reduced nutrient conditions (Thormann et al., 2004). Therefore, to optimize pili expression, initial growth of cultures was in LB media under shaking, aerobic conditions at 30 °C until cells reached mid-logarithmic phase, at which point cells were transferred to low nutrient, minimal media with 0.68 mM CaCl₂ to induce pilin production.

Isolated pili were obtained from cells using methods developed previously for heterologous expression in *E. coli* (Ueki et al., 2020) and *T. thermophilus* (Neuhaus et al., 2020). Pili were sheared from cells in a Waring blender and membrane solubilized, followed by either filtration or ammonium sulfate precipitation. In each instance, pili measuring roughly 3 nm in diameter, similar in morphology to those produced in *Geobacter* (Fig. 2f), were collected. Samples obtained via ammonium sulfate precipitation regularly contained larger amounts of pili, but also were less pure (as determined by SDS gel electrophoresis). A second ammonium sulfate precipitation resulted in preparations with no further distinguishable contamination. Preparations of pili variants showed greater aggregation, which was alleviated by the early addition of EDTA. All samples were treated with deoxyribonuclease (DNase) prior to further analyses.

In order to determine whether the pili isolated from S. oneidensis had characteristics similar to those produced natively by Geobacter, thin-film conductance experiments were carried out (Ueki et al., 2020). Drop cast pili amounts (\sim 20 µg) were magnitudes lower than in previous work (~2000 μg (Ueki et al., 2020)) to avoid hydrogel formation (Ing et al., 2018) and better enable thin-film coating. Concentrated pili samples at \sim 20 µg/µL were drop cast at the center of circular orientation 4-probe arrays of 100 μm lengths and 2 μm gap distances, and air dried for 24 h prior to measurement (Fig. 2g). This differs from the previous methods (Ueki et al., 2020) that used larger nanoelectrode array ladders in a straight line. Pili distribution across electrodes following evaporation/sample drying led to only thin films on the outer edge 4-probe ladders being used for measurements (Fig. S1) which limits direct comparisons to previous literature values from samples that were cast with larger pili amounts at the centers of single, larger 4-probe ladders of different spacing (Ueki et al., 2020).

Wild-type *S. oneidensis* MR-1 pili and wild-type *G. sulfurreducens* pili isolated from *E. coli* (with conductance similar to native *Geobacter* pili) were used for comparisons. As expected, the wild-type *Shewanella* pili showed low electrical activity, while the wild-type *G. sulfurreducens* pili isolated from *S. oneidensis::* 4 had electrical activities similar to those *G. sulfurreducens* pili isolated from *E. coli*, producing similar conductance in response to voltage sweeps (Fig. 2h). However, the heterogeneous, engineered pili, composed of both wild-type and carboxy-terminal extended monomers, demonstrated roughly an order-of-magnitude improvement in conductivity (Fig. 2h), possibly due to side chain charge effects, as previously reported (Malvankar et al., 2015), and potentially to improved electrode contacts, in the case of the cysteine tag. These results are in line with HA-tag extensions previously reported by (Ueki et al., 2020), where it was also demonstrated engineered heterogeneous pili to be more conductive over wild-type.

3.3. Metal-organic filament synthesis

G. sulfurreducens pili have previously been reported to bundle along

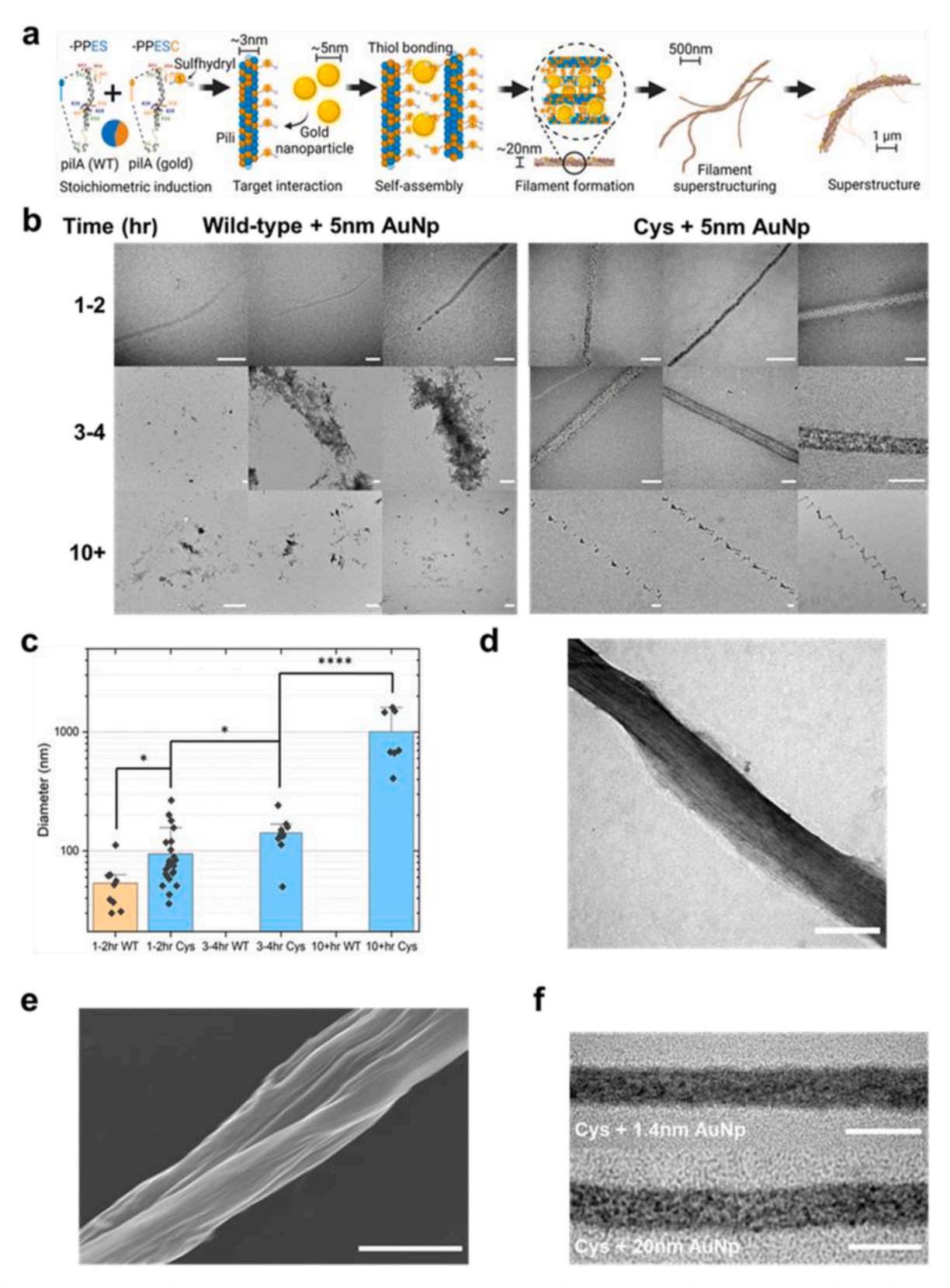


Fig. 3. Pili interactions for metal-organic filaments. (a) Schematic for co-expression of wild-type + mutant PilA monomers assembling into heterogeneous pili designed for specific target interactions, forming long-range filament bundles of conductive pili culminating in superstructures. (b) Assembly monitoring of wild-type & gold binding (Cys) heterogeneous pili with 5 nm gold nanoparticles into filaments, with aliquots from single reaction sample taken over 1-2 h, 3-4 h, and 10+ hrs time. (c) Calculated diameters of sample pili filaments taken over time, performed with paired two sample t-test *p < 0.05, ****p < 0.00005 (d) Gold-binding heterogeneous pili incubated with 5 nm AuNp at a 3 h time point. Stained to highlight individual pili. (e) SEM superstructure of gold-binding heterogeneous pili incubated with 5 nm AuNp at 10+ hrs reaction time. (f) Gold-binding heterogeneous pili incubated with 1.4 and 20 nm AuNp at 3 h time points. Scale bars: 200 nm (b 1-2 h + 3-4 h, d, f); 500 nm (b 10+ hrs); 1 μ m (e). All images used for statistical analyses may be found in Figs. S2-4.

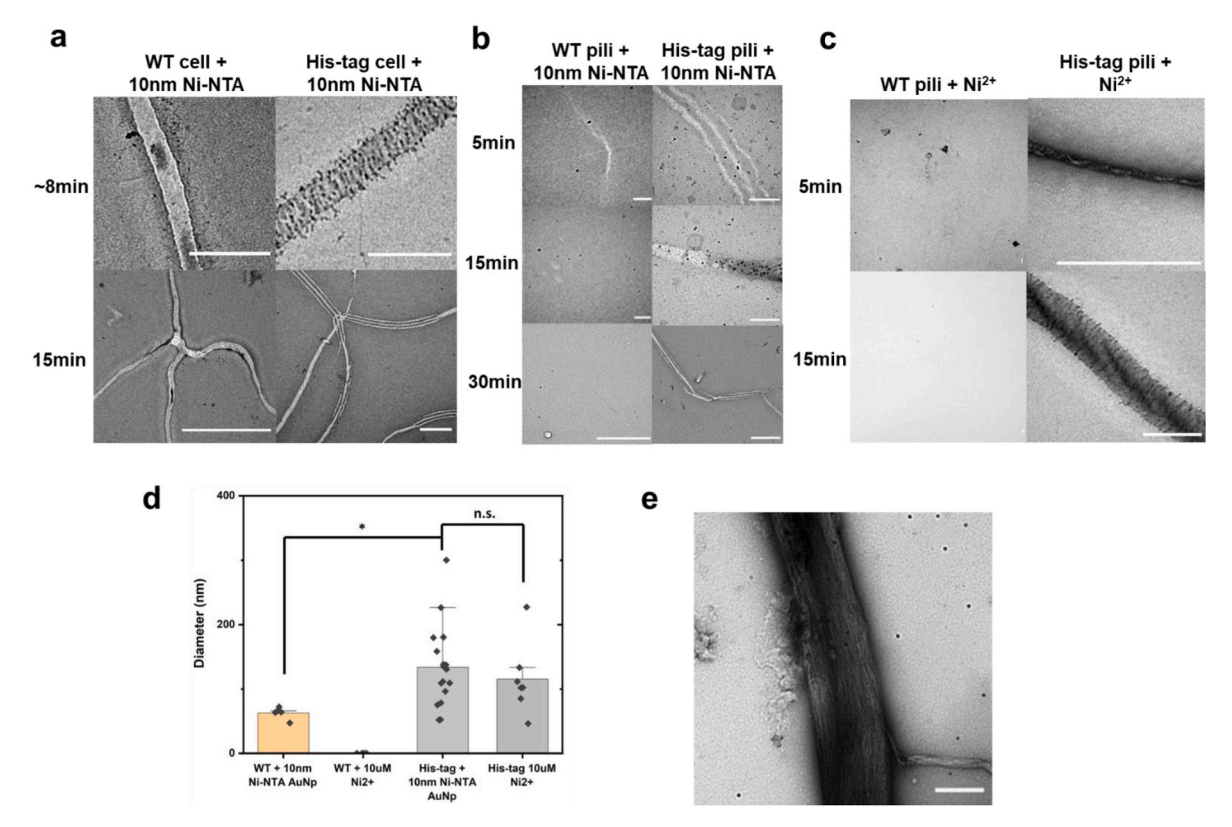


Fig. 4. His-tag interactions into self-assembled filaments. TEM (a) Uninduced (WT), and induced (his-tag, $100 \,\mu\text{M}$ IPTG) *S. oneidensis::* $24 \, \text{pESOpH}$ cells incubated with 10 nm Ni-NTA conjugated gold nanoparticles on ice. Nanoparticles are heavily positioned over surface of induced pili filaments quickly after nanoparticle introduction, while uninduced samples aggregated filaments are devoid of apparent nanoparticle positioning and incorporation. (b) Isolated pili samples interacting with 10 nm Ni-NTA AuNp over time. His-tag samples can be seen incorporating nanoparticles and follow similar structural pattern to formation as expressed on cells, albeit at slower rates most likely due to concentration. (c) Isolated pili samples incubated with free Ni²⁺ ions. Supramolecular filament structuring is present only in his-tag pili samples. (d) Calculated diameters of WT and His-tag pili with Ni-NTA AuNp and free Ni²⁺, performed with paired two sample *t*-test * = p < 0.05; n. s. = not significant. (e) His-tag heterologous pili bound with 10 nm Ni-NTA AuNp at 15 min time point. Stained to highlight individual pili. Scale bars 1 μ m (a, 15min + b, 30min), 200 nm all others. All images used in statistical analysis may be found in Fig. S5.

their lengths (Reguera, 2018; Veazey et al., 2012), therefore, we hypothesized that the addition of the cysteine tag might allow the construction of biohybrid metal:organic structures in which gold nanoparticles served as connectors or interstices between the pili (Fig. 3a). Both wild-type and cysteine-tagged PilA were incubated under buffered acidic conditions (pH 6, ensuring cysteines are reduced) with 5 nm gold nanoparticles overnight. Aliquots from this reaction were taken at a series of time points every hr for the first 4 h and then overnight, placed on gold TEM grids, and negatively stained by uranyl acetate. We find preferential bundling of cysteine-tagged pili occurs over time, until fewer and fewer individual filaments were identified, leaving only visible multi-pili bundles (Fig. 3b). In contrast, bundling of wild-type pili under identical reaction conditions occurs only at early time points (Fig. 3b), and may represent aggregates leftover from shearing from the cell surface (see Fig. 2f). This hypothesis is further supported by the fact that gold nanoparticle dispersion among wild-type pili bundles does not follow any recognizable pattern.

The majority of large, cysteine-mediated bundles (measuring roughly 80 nm in diameter or greater) appeared in the first 2 h of reaction, with average sizes increase to 150 nm in diameter at 4 h (Fig. 3c). After overnight incubation for roughly 10+ hrs filament superstructures measuring near microns in diameter and up to hundreds of microns in length, occasionally taking on a helical appearance, were observed. These superstructures often had smaller sized filaments (10-20 nm diameter) free of visible nanoparticles extending from their surfaces, possibly due to incomplete incorporation via nanoparticle bridging. Closer inspection of cysteine-tagged pili incubated with 5 nm AuNp for 3 h shows a majority of individual pili bundling along their lengths to

create filaments (Fig. 3d). A SEM image of these filaments (Fig. 3e) shows a continuous structure with numerous small filament interactions, a result in good approximation with the schematic representation of pili-nanoparticle interactions outlined in Fig. 3a.

To further validate the hypothesis that creating potential connectors between pili could lead to metal:organic structure formation, we attempted to use different-sized gold nanoparticles to bridge pili. Isolated cysteine-tagged pili were shown to readily form higher order ($\sim 100~\rm nm$ diameter at 2 h) filaments with 5 nm gold nanoparticles (Fig. 2b), as well as 1.4 nm and 20 nm gold nanoparticles (Fig. 3f). Again, no such structures were observed with gold nanoparticle treated wild-type pili controls.

We also assembled pili engineered with histidine tags via bridging with gold nanoparticles (AuNp) surfaced with Ni-NTA (Fig. 4). The histidine-tagged pili also readily formed higher order (200-500 nm diameter) filamentous structures. Cells expressing histidine-tagged pili bound Ni-NTA-coated AuNps and formed structured filaments on their exteriors (Fig. 4a, right), in contrast to cells expressing wild-type pili alone (Fig. 4a, left). Isolated his-tagged pili similarly formed biohybrid structures with 10 nm Ni-NTA AuNp (Fig. 4b) showing similarly patterned assemblies as seen from cells. His-tag pili biohybrid filaments were also found to form in the presence of free nickel ions (Fig. 4c). Although they were smaller in their final diameter (~20-200 nm) than those binding Ni-NTA AuNp, they were still capable of forming structures, whereas the wild-type pilA was not, suggesting the his-tag coordinates with nickel ions to mediate metal:organic structural assemblies. His-tagged filament assembly using either 10 nm Ni-NTA coated gold nanoparticles or free Ni²⁺ ions was analyzed at a 15 min

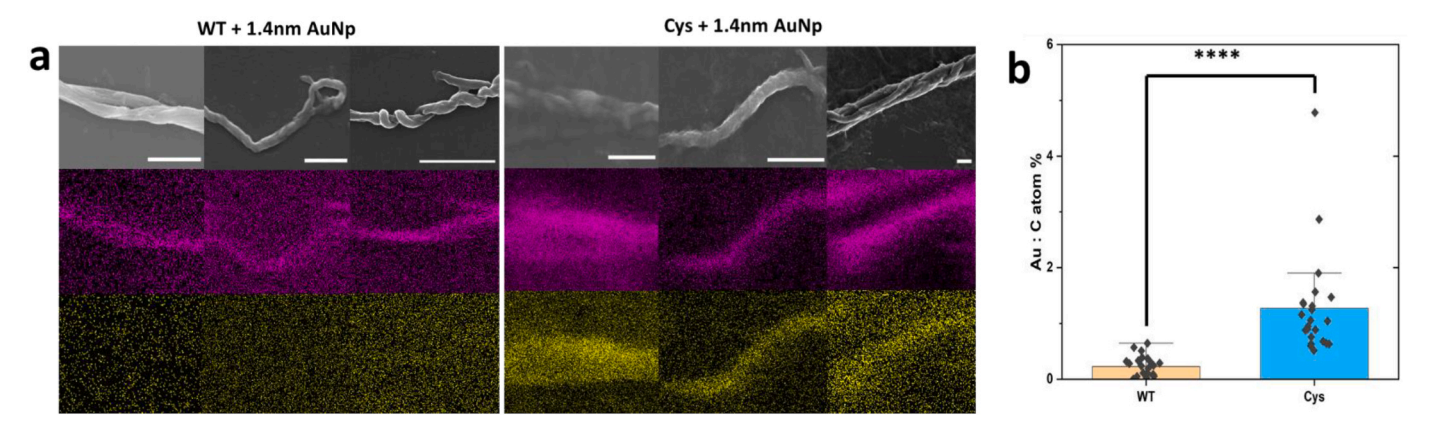


Fig. 5. SEM with energy dispersive X-ray (EDS) overlay data. (a) EDS overlay of three representative gold binding (cys) and wild-type samples following 10 min integration time each. Filament superstructures featuring cysteine sulfhydryl groups for thiol bond formation with gold nanoparticles display heavier gold atom (in yellow) identification at carbon sites (pili, in purple) than those of wild-type. (b) Bar graph from reported EDS atomic percentage data of 23 representative filament samples each of wild-type and cys pili. Cys pili display a significantly higher percentage of gold atoms present in their filament structures than wild-type, in line with representative overlay data and that previously seen in TEM. Samples plated on SiO_2 semiconductive wafers and coated in 1 nm iridium before imaging. Scale bars 5 μ m. Statistical analysis performed by paired two sample t-test, ****p < 0.00005. Raw data used for statistical analysis may be found in Supplementary Figs. S6 and S7.

time point (since His-tag assembly was more rapid than cysteine-tagged assembly; Fig. 4d). Bundling of the His-tagged pili was apparent with nickel alone; no bundling was present for the wild-type. The addition of the gold nanoparticle begins to cause bundling of the wild-type, as was the case for the cysteine-tagged pili (Fig. 3c), but the addition of a Histag improves both the yield and size of aggregates. The individual pili again appear to bundle along their lengths to create filaments (Fig. 4e, compare with Fig. 3d).

3.4. Metal-organic filament composition analysis

To confirm that filaments in fact contained gold nanoparticles, we performed elemental composition experiments using energy dispersive x-ray spectroscopy under SEM. For this, both wild-type and cysteinetagged pili were incubated with 1.4 nm gold nanoparticles for 4 h (identical to reaction conditions for Fig. 3b), and unbound particles were removed by centrifugal filtration. This resulted in high sample concentration and increased filament formation across both samples. The reaction was drop cast onto clean SiO₂ wafers and coated in 1 nm iridium prior to imaging (Fig. 5). The ratio of atomic carbon to gold was used to determine gold nanoparticle incorporation (Fig. 5b). Whereas wild-type filaments had strong carbon signals (purple overlay) that were easily identified, little or no gold signatures were observed (gold overlay; Fig. 5a). The minor gold nanoparticle incorporation observed may result from interactions with carboxyl groups at solvent-exposed terminals (Buglak & Kononov, 2020). In contrast, cysteine-tagged pili showed significant gold incorporation, averaging a ~6x higher ratio of atomic Au:C signature (Fig. 5b). Paired two-sample t-test results from the independent assessment of 46 filaments total (23 each) of both wild-type and cysteine-tagged samples showed a highly significant (p < 0.00005) difference in levels of gold incorporation between filaments.

4. Conclusions

The results demonstrate that conductive filaments comprised of *G. sulfurreducens* pilins can be effectively expressed in *S. oneidensis* and that the pilin protein can be modified to enhance filament conductivity and the fabrication of biohybrid metal:organic structures. Expression pili in *S. oneidensis* enables production under scalable, aerobic conditions and avoids the potential contamination of pilin-based filaments with cytochrome-based filaments that also emanate from *G. sulfurreducens* (Liu et al., 2021). Greater quantities of pili were generated with *S. oneidensis* than from heterologous expression in *E. coli*

(Ueki et al., 2020). Modifying the carboxy termini of the G. sulfurreducens pilin to allow interactions with gold nanoparticles led to the controlled formation of biohybrid filaments. Conductive pili have been composed into electronic devices (Fu et al., 2020; Liu, Fu, et al., 2020; Liu, Gao, et al., 2020), but their random alignment may limit regular microscale assemblies that can be achieved with other electrical biomaterials (Wang et al., 2018). G. sulfurreducens pili have previously been assembled into superstructured bundles (Sun et al., 2021), but that approach required toxic solvents and was difficult to control. Controlled metal:organic assemblies (Brodin et al., 2015; Zhang et al., 2021) coupled with genetic engineering of proteins (Shapiro et al., 2022; Tan et al., 2016; Tan et al., 2017; Ueki et al., 2020) has proven to be a useful avenue for scaling conductive biologics. In a similar vein, genetically engineered, conductive pili may potentially act as key sensor or switching components within self-organized, electrical biomaterials, similar to carbon nanotubes, especially when embedded in nanoscale scaffolds (Sun et al., 2020; Zhang et al., 2020).

Declaration of competing interest

The authors declare that they have no known competing financial interests or personal relationships that could have appeared to influence the work reported in this paper.

Data availability

Data will be made available on request.

Acknowledgements and Funding

This work was supported by the Army Research Office (W911NF-18-1-0169, A.D.E.) and the Welch Foundation (F-1654, A.D.E.). This research was also sponsored by NSF MRSEC IRG-1 under Cooperative Agreement Number DMR-1720595 and the Army Research Laboratory under Cooperative Agreement Number W911NF-17-2-0091. The views and conclusions contained in this document are those of the authors and should not be interpreted as representing the official policies, either expressed or implied, of the Army Research Laboratory or the U.S. Government. The U.S. Government is authorized to reproduce and distribute reprints for Government purposes notwithstanding any copyright notation herein.

TEM was performed with the assistance of Michelle Mikesh at the Center for Biomedical Research Support Microscopy and Imaging Facility at UT Austin (RRID# SCR 021756).

Appendix A. Supplementary data

Supplementary data to this article can be found online at https://doi.org/10.1016/j.bios.2022.114993.

References

- Adhikari, R.Y., Malvankar, N.S., Tuominen, M.T., Lovley, D.R., 2016. Conductivity of individual Geobacter pili. RSC Adv. 6 (10), 8354–8357. https://doi.org/10.1039/ c5ra28092c.
- Banin, E., Brady, K.M., Greenberg, E.P., 2006. Chelator-induced dispersal and killing of Pseudomonas aeruginosa cells in a biofilm. Appl. Environ. Microbiol. 72 (3), 2064–2069. https://doi.org/10.1128/AEM.72.3.2064-2069.2006.
- Bhadra, S., Nguyen, V., Torres, J.-A., Kar, S., Fadanka, S., Gandini, C., Akligoh, H., Paik, I., Maranhao, A.C., Molloy, J., Ellington, A.D., 2021. Producing molecular biology reagents without purification. PLoS One 16 (6), e0252507. https://doi.org/ 10.1371/journal.pone.0252507.
- Bouhenni, R.A., Vora, G.J., Biffinger, J.C., Shirodkar, S., Brockman, K., Ray, R., Wu, P., Johnson, B.J., Biddle, E.M., Marshall, M.J., Fitzgerald, L.A., Little, B.J., Fredrickson, J.K., Beliaev, A.S., Ringeisen, B.R., Saffarini, D.A., 2010. The role of Shewanella oneidensis MR-1 outer surface structures in extracellular electron transfer. Electroanalysis 22 (7–8), 856–864. https://doi.org/10.1002/elan.200880006.
- Brodin, J.D., Smith, S.J., Carr, J.R., Tezcan, F.A., 2015. Designed, helical protein nanotubes with variable diameters from a single building block. J. Am. Chem. Soc. 137 (33), 10468–10471. https://doi.org/10.1021/jacs.5b05755.
- Brown, S., 1997. Metal-recognition by repeating polypeptides. Nat. Biotechnol. 15 (3), 269–272. https://doi.org/10.1038/nbt0397-269.
- Buglak, A.A., Kononov, A.I., 2020. Comparative study of gold and silver interactions with amino acids and nucleobases. RSC Adv. 10 (56), 34149–34160. https://doi.org/ 10.1039/d0ra06486f.
- Corts, A.D., Thomason, L.C., Gill, R.T., Gralnick, J.A., 2019. Efficient and precise genome editing in *Shewanella* with recombineering and CRISPR/Cas9-Mediated counterselection. ACS Synth. Biol. 8 (8), 1877–1889. https://doi.org/10.1021/ acssynbio.9b00188.
- Dundas, C.M., Walker, D.J.F., Keitz, B.K., 2020. Tuning extracellular electron transfer by Shewanella oneidensis using transcriptional logic gates. ACS Synth. Biol. 9 (9), 2301–2315. https://doi.org/10.1021/acssynbio.9b00517.
- Fu, T., Liu, X., Gao, H., Ward, J.E., Liu, X., Yin, B., Wang, Z., Zhuo, Y., Walker, D.J.F., Joshua Yang, J., Chen, J., Lovley, D.R., Yao, J., 2020. Bioinspired bio-voltage memristors. Nat. Commun. 11 (1) https://doi.org/10.1038/s41467-020-15759-y.
- Giltner, C.L., Nguyen, Y., Burrows, L.L., 2012. Type IV pilin proteins: versatile molecular modules. Microbiol. Mol. Biol. Rev. 76 (4), 740–772. https://doi.org/10.1128/ MMBR.00035-12.
- Ing, N.L., Spencer, R.K., Luong, S.H., Nguyen, H.D., Hochbaum, A.I., 2018. Electronic conductivity in biomimetic α-helical peptide nanofibers and gels. ACS Nano 12 (3), 2652–2661. https://doi.org/10.1021/acsnano.7b08756.
- Liu, X., Fu, T., Ward, J., Gao, H., Yin, B., Woodard, T., Lovley, D.R., Yao, J., 2020a. Multifunctional protein nanowire humidity sensors for green wearable electronics. Advanced Electronic Materials 6 (9), 2000721. https://doi.org/10.1002/aelm.202000721.
- Liu, X., Gao, H., Ward, J.E., Liu, X., Yin, B., Fu, T., Chen, J., Lovley, D.R., Yao, J., 2020b. Power generation from ambient humidity using protein nanowires. Nature 578 (7796), 550–554. https://doi.org/10.1038/s41586-020-2010-9.
- Liu, X., Walker, D.J.F., Nonnenmann, S.S., Sun, D., Lovley, D.R., 2021. Direct observation of electrically conductive pili emanating from Geobacter sulfurreducens. mBio 12 (4), e0220921. https://doi.org/10.1128/mBio.02209-21.
- Lovley, D.R., Walker, D.J.F., 2010. Geobacter protein nanowires. Frontiers in Microbiology 10. https://doi.org/10.3389/fmicb.2019.02078.
 Malvankar, N.S., Vargas, M., Nevin, K., Tremblay, P.L., Evans-Lutterodt, K.,
- Malvankar, N.S., Vargas, M., Nevin, K., Tremblay, P.L., Evans-Lutterodt, K., Nykypanchuk, D., Martz, E., Tuominen, M.T., Lovley, D.R., 2015. Structural basis for metallic-like conductivity in microbial nanowires. mBio 6 (2), e00084. https://doi. org/10.1128/mBio.00084-15.
- McCarter, L.L., 2001. Polar flagellar motility of the *vibrionaceae*. Microbiol. Mol. Biol. Rev. 65 (3), 445–462. https://doi.org/10.1128/mmbr.65.3.445-462.2001.
- McLean, J.S., Pinchuk, G.E., Geydebrekht, O.V., Bilskis, C.L., Zakrajsek, B.A., Hill, E.A., Saffarini, D.A., Romine, M.F., Gorby, Y.A., Fredrickson, J.K., Beliaev, A.S., 2008. Oxygen-dependent autoaggregation in Shewanella oneidensis MR-1. Environ. Microbiol. 10 (7), 1861–1876. https://doi.org/10.1111/j.1462-2920.2008.01608.x.
- Muskovich, M., Bettinger, C.J., 2012. Biomaterials-based electronics: polymers and interfaces for biology and medicine. Advanced Healthcare Materials 1 (3), 248–266. https://doi.org/10.1002/adhm.201200071.
- Neuhaus, A., Selvaraj, M., Salzer, R., Langer, J.D., Kruse, K., Kirchner, L., Sanders, K., Daum, B., Averhoff, B., Gold, V.A.M., 2020. Cryo-electron microscopy reveals two distinct type IV pili assembled by the same bacterium. Nat. Commun. 11 (1) https://doi.org/10.1038/s41467-020-15650-w.
- Pirbadian, S., Barchinger, S.E., Leung, K.M., Byun, H.S., Jangir, Y., Bouhenni, R.A., Reed, S.B., Romine, M.F., Saffarini, D.A., Shi, L., Gorby, Y.A., Golbeck, J.H., El-

- Naggar, M.Y., 2014. Shewanella oneidensis MR-1 nanowires are outer membrane and periplasmic extensions of the extracellular electron transport components. Proc. Natl. Acad. Sci. USA 111 (35), 12883–12888. https://doi.org/10.1073/pnas.1410551111.
- Reguera, G., 2018. Harnessing the power of microbial nanowires. Microb. Biotechnol. 11 (6), 979–994. https://doi.org/10.1111/1751-7915.13280.
- Reguera, G., McCarthy, K.D., Mehta, T., Nicoll, J.S., Tuominen, M.T., Lovley, D.R., 2005. Extracellular electron transfer via microbial nanowires. Nature 435 (7045), 1098–1101. https://doi.org/10.1038/nature03661.
- Rosenbaum, M.A., Bar, H.Y., Beg, Q.K., Segrè, D., Booth, J., Cotta, M.A., Angenent, L.T., 2012. Transcriptional analysis of Shewanella oneidensis MR-1 with an electrode compared to Fe(III)citrate or oxygen as terminal electron acceptor. PLoS One 7 (2), e30827. https://doi.org/10.1371/journal.pone.0030827.
- Saville, R.M., Dieckmann, N., Spormann, A.M., 2010. Spatiotemporal activity of the mshA gene system in Shewanella oneidensis MR-1 biofilms. FEMS (Fed. Eur. Microbiol. Soc.) Microbiol. Lett. 308 (1), 76–83. https://doi.org/10.1111/j.1574-6968.2010.01995.x.
- Shapiro, D.M., Mandava, G., Yalcin, S.E., Arranz-Gibert, P., Dahl, P.J., Shipps, C., Gu, Y., Srikanth, V., Salazar-Morales, A.I., O'Brien, J.P., Vanderschuren, K., Vu, D., Batista, V.S., Malvankar, N.S., Isaacs, F.J., 2022. Protein nanowires with tunable functionality and programmable self-assembly using sequence-controlled synthesis. Nat. Commun. 13 (1) https://doi.org/10.1038/s41467-022-28206-x.
- Steidl, R.J., Lampa-Pastirk, S., Reguera, G., 2016. Mechanistic stratification in electroactive biofilms of Geobacter sulfurreducens mediated by pilus nanowires. Nat. Commun. 7 (1), 12217 https://doi.org/10.1038/ncomms12217.
- Sun, W., Shen, J., Zhao, Z., Arellano, N., Rettner, C., Tang, J., Cao, T., Zhou, Z., Ta, T., Streit, J.K., Fagan, J.A., Schaus, T., Zheng, M., Han, S.J., Shih, W.M., Maune, H.T., Yin, P., 2020. Precise pitch-scaling of carbon nanotube arrays within three-dimensional DNA nanotrenches. Science 368 (6493), 874–877. https://doi.org/10.1126/science.aaz7440.
- Sun, Y.-L., Montz, B.J., Selhorst, R., Tang, H.-Y., Zhu, J., Nevin, K.P., Woodard, T.L., Ribbe, A.E., Russell, T.P., Nonnenmann, S.S., Lovley, D.R., Emrick, T., 2021. Solventinduced assembly of microbial protein nanowires into superstructured bundles. Biomacromolecules 22 (3), 1305–1311. https://doi.org/10.1021/acs. biomac.0c01790.
- Suzuki, Y., Kouzuma, A., Watanabe, K., 2020. CRISPR/Cas9-mediated genome editing of Shewanella oneidensis MR-1 using a broad host-range pBBR1-based plasmid. J. Gen. Appl. Microbiol. 66 (1), 41–45. https://doi.org/10.2323/jgam.2019.04.007.
- Tan, Y., Adhikari, R.Y., Malvankar, N.S., Pi, S., Ward, J.E., Woodard, T.L., Nevin, K.P., Xia, Q., Tuominen, M.T., Lovley, D.R., 2016. Synthetic biological protein nanowires with high conductivity. Small 12 (33), 4481–4485. https://doi.org/10.1002/smll.201601112.
- Tan, Y., Adhikari, R.Y., Malvankar, N.S., Ward, J.E., Woodard, T.L., Nevin, K.P., Lovley, D.R., 2017. Expressing the geobacter metallireducens PilA in geobacter sulfurreducens yields pill with exceptional conductivity. mBio 8 (1). https://doi.org/ 10.1128/mBio.02203-16.
- Thormann, K.M., Saville, R.M., Shukla, S., Pelletier, D.A., Spormann, A.M., 2004. Initial Phases of biofilm formation in Shewanella oneidensis MR-1. J. Bacteriol. 186 (23), 8096–8104. https://doi.org/10.1128/JB.186.23.8096-8104.2004.
- Ueki, T., Nevin, K.P., Rotaru, A.E., Wang, L.Y., Ward, J.E., Woodard, T.L., Lovley, D.R., 2018. Geobacter strains expressing poorly conductive pili reveal constraints on direct interspecies electron transfer mechanisms. mBio 9 (4). https://doi.org/ 10.1128/mBio.01273-18
- Ueki, T., Walker, D.J.F., Woodard, T.L., Nevin, K.P., Nonnenmann, S.S., Lovley, D.R., 2020. An Escherichia coli chassis for production of electrically conductive protein nanowires. ACS Synth. Biol. 9 (3), 647–654. https://doi.org/10.1021/ prographic.0100506.
- Vargas, M., Malvankar, N.S., Tremblay, P.L., Leang, C., Smith, J.A., Patel, P., Snoeyenbos-West, O., Nevin, K.P., Lovley, D.R., 2013. Aromatic amino acids required for pili conductivity and long-range extracellular electron transport in Geobacter sulfurreducens. mBio 4 (2). https://doi.org/10.1128/mBio.00105-13 e00105-00113
- Veazey, J.P., Reguera, G., Tessmer, S.H., 2012. Erratum: electronic properties of conductive pili of the metal-reducing bacterium *Geobacter sulfurreducens* probed by scanning tunneling microscopy [Phys. Rev. E84. Phys. Rev. 85 (4), 060901 https:// doi.org/10.1103/physreve.85.049907, 2011.
- Walker, D.J.F., Martz, E., Holmes, D.E., Zhou, Z., Nonnenmann, S.S., Lovley, D.R., 2019. The archaellum of methanospirillum hungatei Is electrically conductive. mBio 10 (2), e00579–19. https://doi.org/10.1128/mBio.00579-19.
- Wang, S., Xu, J., Wang, W., Wang, G.-J.N., Rastak, R., Molina-Lopez, F., Chung, J.W., Niu, S., Feig, V.R., Lopez, J., Lei, T., Kwon, S.-K., Kim, Y., Foudeh, A.M., Ehrlich, A., Gasperini, A., Yun, Y., Murmann, B., Tok, J.B.H., Bao, Z., 2018. Skin electronics from scalable fabrication of an intrinsically stretchable transistor array. Nature 555 (7694), 83–88. https://doi.org/10.1038/nature25494.
- Zhang, L.T., Zhou, Y., Han, S.T., 2021. The role of metal–organic frameworks in electronic sensors. Angew. Chem. Int. Ed. 60 (28), 15192–15212. https://doi.org/10.1002/anie.202006402.
- Zhang, Y., Mao, X., Li, F., Li, M., Jing, X., Ge, Z., Wang, L., Liu, K., Zhang, H., Fan, C., Zuo, X., 2020. Nanoparticle-assisted alignment of carbon nanotubes on DNA origami. Angew. Chem. Int. Ed. 59 (12), 4892–4896. https://doi.org/10.1002/anie.201916043.